Direct Measurement of Helicoid Surface States in RhSi Using Nonlinear Optics

Dylan Rees,[1,2,*] Baozhu Lu,[3,*] Yue Sun,[2,4] Kaustuv Manna,[5,6] Rüstem Özgür,[7] Sujan Subedi,[3] Horst Borrmann,[5] Claudia Felser,[5] J. Orenstein,[1,2,†] and Darius H. Torchinsky[3,‡]

[1]*Department of Physics, University of California, Berkeley, Berkeley, California 94720, USA*
[2]*Materials Science Division, Lawrence Berkeley National Laboratory, Berkeley, California 94720, USA*
[3]*Department of Physics, Temple University, Philadelphia, Pennsylvania 19122, USA*
[4]*Department of Chemistry, University of California, Berkeley, Berkeley, California 94720, USA*
[5]*Max Planck Institute for Chemical Physics of Solids, Dresden D-01187, Germany*
[6]*Department of Physics, Indian Institute of Technology Delhi, New Delhi 110016, India*
[7]*Department of Materials Science and Engineering, University of California, Berkeley, California 94720, USA*

(Received 9 March 2021; revised 2 August 2021; accepted 15 September 2021; published 8 October 2021)

Despite the fundamental nature of the edge state in topological physics, direct measurement of electronic and optical properties of the Fermi arcs of topological semimetals has posed a significant experimental challenge, as their response is often overwhelmed by the metallic bulk. However, laser-driven currents carried by surface and bulk states can propagate in different directions in nonsymmorphic crystals, allowing for the two components to be easily separated. Motivated by a recent theoretical prediction G. Chang *et al.*, Phys. Rev. Lett. **124**, 166404 (2020), we have measured the linear and circular photogalvanic effect currents deriving from the Fermi arcs of the nonsymmorphic, chiral Weyl semimetal RhSi over the 0.45–1.1 eV incident photon energy range. Our data are in good agreement with the predicted spectral shape of the circular photogalvanic effect as a function of photon energy, although the direction of the surface photocurrent departed from the theoretical expectation over the energy range studied. Surface currents arising from the linear photogalvanic effect were observed as well, with the unexpected result that only two of the six allowed tensor element were required to describe the measurements, suggesting an approximate emergent mirror symmetry inconsistent with the space group of the crystal.

DOI: 10.1103/PhysRevLett.127.157405

A universal property of topological matter is the existence of a protected edge state, e.g., the current-carrying edge state of the quantum Hall effect [1,2] or the spin-momentum locked surface states of bulk topological insulators [3,4]. In topological Weyl semimetals, which host emergent massless, chiral charge carriers called Weyl fermions, the topological edge state comprises open Fermi surface arcs formed of helicoidally dispersing, spin-momentum locked quasiparticles that are constrained to the sample surface [5,6]. The arcs connect the projections of opposite chirality Weyl nodes, curving in complementary shapes on the 2D surface Brillouin zones on the opposite sides of the crystal. The existence of these states has been confirmed by ARPES [7–10] and quasiparticle interference measurements [11] and have been shown to play a central role in quantum oscillations [12,13]. However, despite a number of predictions focused on the role of the Fermi arcs in topological semimetal physics [14–19], their transport and optical properties have largely remained hidden, as they are often dominated by bulk response functions. For example, experiments aimed at measuring the linear conductivity of surface states run into difficulties because of shorting by the metallic bulk that lies below.

In this Letter we demonstrate experimentally that the second-order nonlinear conductivity, which describes the strength and symmetry of the photogalvanic effects (PGEs), provides a means to selectively probe surface state electronic properties in Weyl semimetals. The PGEs are phenomena in which optical excitation generates a dc current that arises from intrinsic breaking of inversion symmetry, rather than applied bias voltage or inhomogeneous doping [20,21]. A further defining property of PGEs is sensitivity of the direction of photocurrent, $\mathbf{J}$, to the polarization state of the optical electric field $\mathbf{E}$, as described by the phenomenological relation

$$J_i = \gamma_{ijk} E_j E_k + i\beta_{ij}(\mathbf{E} \times \mathbf{E}^*)_j. \tag{1}$$

The first term on the right-hand side of Eq. (1) describes a current generated by linearly polarized light (the LPGE) in terms of the polar tensor γ_{ijk}. The second term corresponds to a photocurrent whose direction reverses with reversal of the helicity of the photoexcitation. This circular PGE (CPGE) is proportional to the axial tensor β_{ij}. Both PGE response tensors are zero in the presence of inversion symmetry.

The CPGE has received particular attention in the Weyl semimetal RhSi and related topological semimetals, because they crystallize in structures in which all mirror symmetries are broken, forming a chiral (or handed) medium [22–38]. In chiral Weyl semimetals, nodes with opposite topological charge need not be degenerate in energy allowing for one node to lie near the Fermi energy E_F while its oppositely charged partner may be well below [30,39–41]. The breaking of degeneracy creates a photon energy window in which CPGE arises exclusively from the node near E_F, theoretically allowing a quantized CPGE to emerge with amplitude directly proportional to its Berry monopole charge [39]. However, recent experiments with light incident on the (111) surface of RhSi and related isostructural compounds have shown that ideal quantization of the CPGE is disrupted by optical transitions between non-Weyl bands that lie within the quantization window [42,43]. Nevertheless, it was also shown that the polarization selection rules for both CPGE and LPGE observed on (111) faithfully follow constraints imposed by the symmetry of the bulk [42]. As we show below, these constraints provide a route to selectively probe the Fermi arc surface states on the (001) surface.

The space group of RhSi (#198) contains two operations: a threefold rotation about the [111] direction and a nonsymmorphic screw symmetry in which a twofold rotation about the z axis is combined with a translation by $(1/2, 0, 1/2)$ [Figs. 1(a) and 1(b)]. In describing bulk response functions, where perfect translational symmetry is assumed, the screw operation imposes the same constraints on response tensors as twofold rotation. The combination of the three- and twofold rotational symmetry greatly reduces the number of nonvanishing elements of the γ_{ijk} and β_{ij} tensors that describe the bulk PGE response. Only tensor elements $\gamma_{xyz} = \gamma_{yzx} = \gamma_{zxy}$ of the LPGE response are nonzero, and the CPGE tensor is purely diagonal with $\beta_{ij} = \beta\delta_{ij}$. Note that given the reduction of the CPGE tensor to a scalar, Eq. (1) predicts that the CPGE current flows parallel to the wave vector of excitation light, independent of the crystal orientation.

As mentioned above, previous studies with light incident on the (111) surface verified the symmetry-based predictions for the bulk response functions [42]. Specifically, the CPGE signal was below the noise level at normal incidence, consistent with the prediction that it flows parallel to the optical wave vector and therefore does not radiate in the direction of specular reflection [Fig. 1(c)]. As further confirmation, THz radiation from CPGE current 2 orders of magnitude above the noise level was observed when the angle of incidence was set 45° from the normal direction, where the bulk symmetry and measurement geometry imply a radiating CPGE current parallel to the surface.

The experiments described below were stimulated by the prediction that the photogalvanic response to light normally incident on the (001) surface would be qualitatively different than (111), directly revealing the presence of topologically protected surface states through the observation of a surface current [44]. Note that for (001) the symmetry of the bulk predicts that LPGE as well as CPGE current flows normal to the surface (see the Supplemental Material [45]), in which case no radiation from PGEs is expected, as with CPGE on the (111) surface. The crucial ingredient leading to the prediction of PGE currents parallel to the (001) is the presence of a screw symmetry in the space group. Truncation of the crystal at (001) disrupts the translational component of the screw operation and violates the effective twofold symmetry. Consequently there is no operation, other than the identity, that transforms the (001) surface to

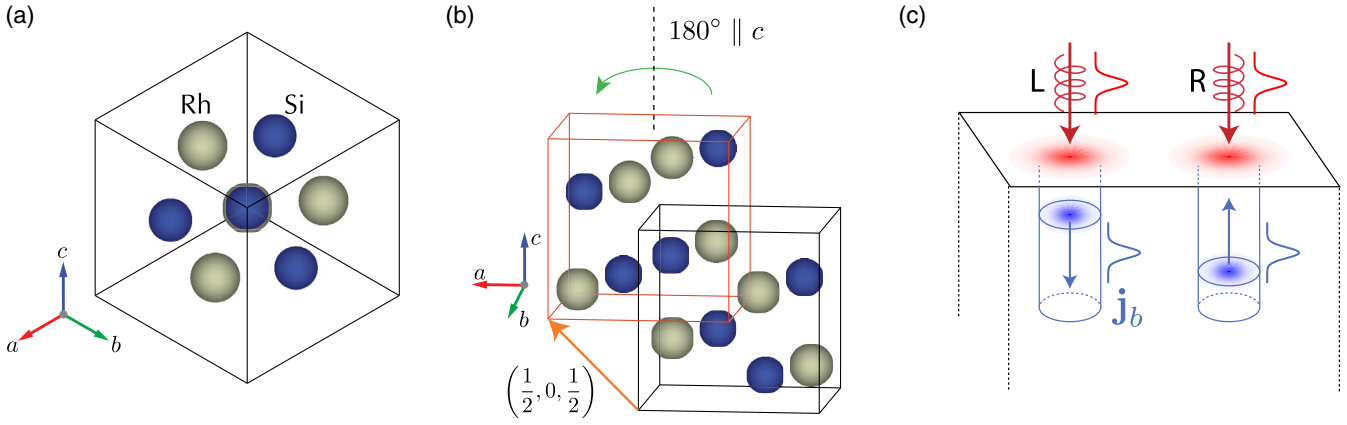

FIG. 1. (a) Unit cell displayed with the [111] direction pointing out of the page, showing the threefold rotational symmetry of the crystal. (b) Extended RhSi structure, showing two alternate unit cells (black and orange). When the unit cell marked by the black frame is rotated by 180° about the z axis and displaced by $(1/2, 0, 1/2)$, it is identical to the unit cell marked by the orange frame, illustrating the twofold screw symmetry. (c) When circularly polarized light is incident on RhSi, the bulk CPGE current will be directed perpendicular to the surface, with its sign determined by the incident light's handedness. L and R refer to left- and right-handed circular polarization, and $\mathbf{j}_b$ refers to the bulk CPGE current.

itself, and all tensor elements disallowed by bulk symmetry become allowed for surface-localized electronic states. In particular the six elements with only x and y indices (i.e., γ_{xxx}, γ_{xxy}, γ_{xyy}, γ_{yxx}, γ_{yxy}, and γ_{yyy}) are not forbidden, allowing for in plane photocurrent and specular THz radiation to be generated by light at normal incidence.

The apparatus used to observe short-lived surface currents via their THz radiation is shown in Fig. 2(a). The excitation source was an optical parametric amplifier pumped by an amplified Ti:Sapphire laser, producing wavelength tunable pulses from 1150–2600 nm (0.48–1.1 eV) and pulse duration ≈100 fs. In plane photogalvanic currents radiated a THz pulse into free space that was focused onto a ZnTe crystal for time-resolved electro-optic sampling of the THz transient (whereas the radiation due to through plane bulk photocurrents did not emerge from the sample) [42]. The experimental setup is discussed in more detail in the Supplemental Material which includes Refs. [46,47].

Figures 2(b) and 2(c) show the experimental configurations used to measure the direction of the PGE currents for different polarization states of the normally incident radiation. The incident light was chosen to be either left or right circularly polarized, or linearly polarized with the plane of polarization rotatable through an angle θ [Fig. 2(b)]. In addition, the sample was also rotated about the optic axis by an angle ϕ [Fig. 2(c)]. The crystal axes were determined by

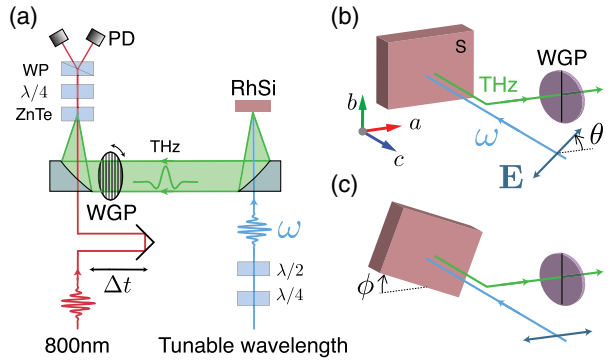

FIG. 2. (a) Schematic of experiment used to detect photogalvanic currents in RhSi via terahertz detection. Near infrared light with tunable wavelength and polarization is focused onto the [001] RhSi surface at normal incidence. Terahertz radiation is collected and collimated using off-axis parabolic mirrors. It passes through a wire-grid polarizer before being focused onto a ZnTe crystal. Light with $\lambda = 800$ nm and variable time delay Δt copropagates through the ZnTe for electro-optical detection of the terahertz. PD, photodiode; WP, Wollaston prism; WGP wire-grid polarizer; $\lambda/2$, half-wave plate; $\lambda/4$, quarter-wave plate. (b) In one experimental configuration, the sample is kept fixed while the pump polarization is rotated by angle θ. The sample axes are set such that [100] and [010] are horizontal and vertical in the lab frame respectively. (c) In the second configuration, the pump polarization is fixed at $\theta = 0$, and the sample is rotated by an angle ϕ.

Laue diffraction and the sample rotation stage was initialized such that at $\phi = 0$ (100) and (010) crystal axes are horizontal and vertical in the laboratory reference frame, respectively (see the Supplemental Material [45]). Samples from two different batches were used in our experiments. A Flack parameter of $-0.06(4)$ was measured for both samples, indicating a very high enantiomeric purity [48,49]. Further information on the (001) oriented RhSi samples used here can also be found in the Supplemental Material [45].

Figure 3(a) shows direct evidence for the generation of in plane helicity-dependent photocurrent at normal incidence on the (001) surface. The THz amplitude plotted on the vertical axis is the difference in radiation generated by left and right circularly polarized light $\hbar\omega = 0.8$ eV and is thus a measure of the CPGE. The two plots show the dependence of the horizontal (H) and vertical (V) components of the CPGE amplitude on the angle of rotation ϕ of the sample about the optic axis. The fact that CPGE is observable at normal incidence already suggests that in plane photocurrent is generated. As Fig. 3(b) illustrates, the dipole radiation pattern for normally directed photocurrent has a node at the angle of specular reflection from the surface and therefore does not directly generate THz radiation, although weaker radiation from multiple scattering is possible. The proof that the observed radiation does indeed arise from an in plane CPGE current is the dependence of the H and V components of the CPGE radiation on ϕ. The solid lines in Fig. 3(a) are fits to $A\cos(\phi - \phi_0)$ and $A\sin(\phi - \phi_0)$, with $\phi_0 \approx 10°$ for both components. This dependence of the CPGE amplitude on ϕ proves that as the sample rotates the CPGE current rotates as well, maintaining an angle ϕ_0 with respect to the [100] direction. This behavior is in contrast to a normally directed CPGE current, which would be independent of ϕ.

Having shown that a CPGE surface current is observed in violation of the restrictions placed by the symmetry of the bulk, we next tested the theoretical prediction for the

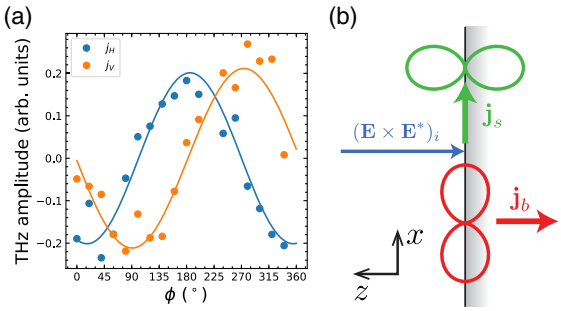

FIG. 3. (a) Amplitude of CPGE for horizontally and vertically polarized THz emission as a function of sample orientation ϕ. (b) Schematic showing directions of bulk PGE ($\mathbf{j}_b$, red) and surface PGE ($\mathbf{j}_s$, green) with normally incident light on the 001 surface of RhSi with the resulting radiation patterns. In general $\mathbf{j}_s$ has a component in x and y.

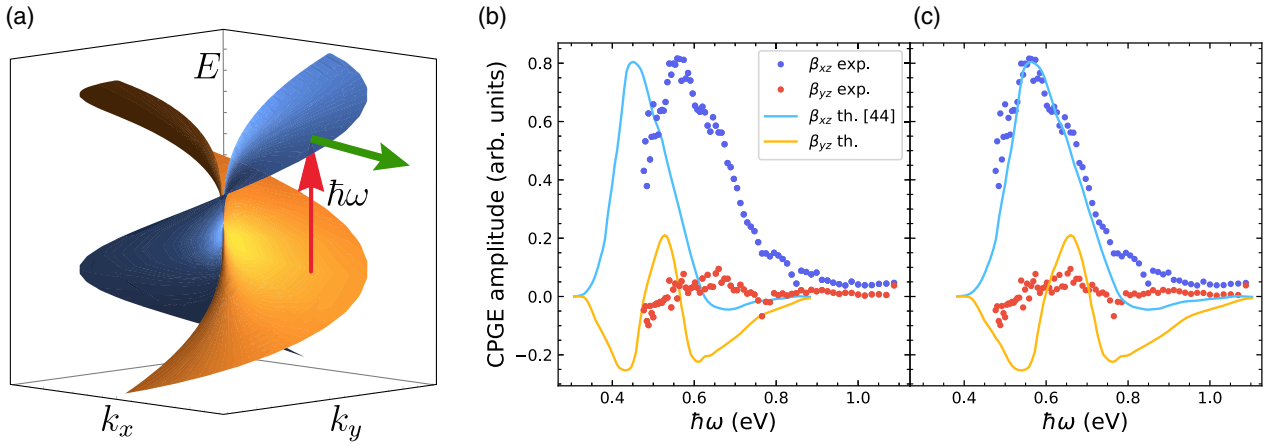

FIG. 4. (a) Schematic of surface helicoid bands including a photoexcitation of an electron at energy $\hbar\omega$ (red arrow) and the induced current (green arrow). (b) CPGE spectral data for β_{xz} and β_{yz} compared with theory from Ref. [44]. (c) Experimental data compared with theory after rescaling of energy. Rescaling of the energy by a factor of 1.25 is seen when density functional theory - local density approximation theory is augmented by inclusion of a certain amount of Hartree-Fock exchange using hybrid density functionals, for example in the Heyd, Scuseria, and Ernzerhof approach.

dependence of CPGE amplitude and direction on $\hbar\omega$. The surface bands responsible for Fermi arcs in RhSi comprise two intertwined helicoids with opposite spin polarization, as illustrated schematically in Fig. 4(a) in a plot of energy vs in plane momentum [30,50]. The helicity-dependent in plane CPGE current arises from spin-flip optical transitions between the two helicoids, as indicated by the arrows in Fig. 4(a).

The comparison of theoretical and experimental measured spectra shown in Figs. 4(b) and 4(c) strongly implicates transitions involving Fermi arc states as the origin of the CPGE effect at the (001) surface. Figure 4(b) compares the observed CPGE amplitude (closed circles) as a function of ω with the spectra predicted using Wannier functions derived from first principles calculations (solid lines) [44]. The two curves in Fig. 4(b) correspond to the H and V components of the CPGE current, proportional to β_{xz} and β_{yz}, respectively. The spectra were uniformly consistent between multiple points on the surfaces of the two samples studied. See the Supplemental Material for more data. Figure 4(c) shows that the evident discrepancy between theoretical prediction and experiment is resolved to a remarkable extent when the energy axis is scaled by a factor of 1.25. Such an increase in the energy of optical transitions can be found when screening effects beyond the local density approximation are considered [51].

To fully characterize the nonlinear response, we measured the response to linear polarization, i.e., LPGE, in addition to the CPGE. Although Ref. [44] did not provide theoretical predictions for the LPGE, the implication of that work is that since twofold rotational symmetry is broken at the surface, the six elements of γ_{ijk} that contain only x and y indices, forbidden in the bulk response, become allowed at the (001) surface. This symmetry-based argument would then predict the existence of in plane LPGE currents whose directions need not correlate or align with the cubic axes of the crystal.

As was the case with circularly polarized light, THz radiation was readily observed at normal incidence under photoexcitation with linearly polarized light. To determine the components of the LPGE tensor we resolved the THz amplitude into the H and V channels, varying the polarization angle of the pump beam while keeping the sample fixed. Figure 5(a) shows the amplitude of the H and V components as a function of the angle of linear polarization, θ. The solid lines are fits to $A\cos[2\theta - \theta_0] + B$. The six independently determined parameters, i.e., the amplitude of the cosine component, A, offset angle θ_0, and offset amplitude B for the H and V channels, are sufficient to determine the relative amplitude of all six elements of γ_{ijk} that contribute to an in plane current at normal incidence (see the Supplemental Material [45]).

Figure 5(b) shows the relative amplitude of the six elements of γ_{ijk} (normalized to γ_{yxx}) in the photon energy

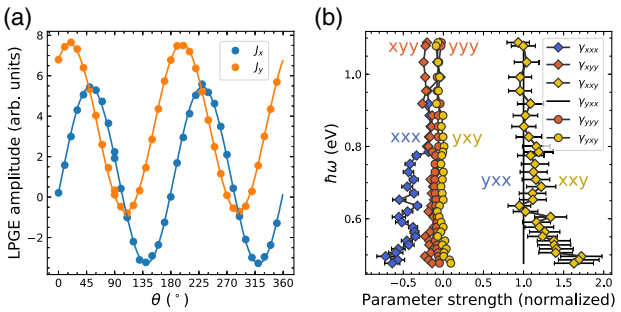

FIG. 5. (a) Terahertz amplitude along x and y as a function of linear pump polarization angle θ for $\lambda = 2000$ nm. (b) Results of fitting data in (a) to general LPGE tensor γ_{ijk}.

range from 0.5 to 1.2 eV, along with error bars deriving from systematic errors discussed in the Supplemental Material [45]. A striking feature of the spectra is that the response at photon energies above ~0.6 eV is dominated by two approximately equal components $\gamma_{yxx} \approx \gamma_{xxy}$ with the other four close to zero, despite the fact that all six tensor components are in principle symmetry allowed. We note that the vanishing of components with an odd number of x indices would suggest a mirror symmetry $x \to -x$ (see the Supplemental Material [45]). A CPGE current directed along the x axis would be consistent with this symmetry. While the components appear to approximately obey such a symmetry, we know of no mechanism which would enforce this. AFM measurements also revealed no patterns in surface topography that could affect the amplitude of photocurrents (see the Supplemental Material [45]).

In conclusion, our measurements provide strong evidence in support of the prediction [44] of a new path to selective probing of the topological surface states in Weyl semimetals. We have observed linear and circular photogalvanic effects that arise selectively from surface states in chiral RhSi by choosing a configuration in which the response of the bulk is forbidden by symmetry. The CPGE spectrum, after a 25% rescaling of the energy axis, showed striking agreement with the response predicted for transitions between the spin polarized helicoidal bands that give rise to Fermi arcs [44]. LPGE measurements also probed the nonlinear response of surface states. An unanticipated result was that over a broad photon energy range only two elements of the nonlinear response tensor γ_{ijk} were required to fit the data, despite the six potentially nonzero elements expected by the C_1 surface symmetry. This result presents a challenge to theory of surface states in Weyl semimetals. Finally, the measurement scheme demonstrated here offers a general approach to selectively probe surface states of topological matter through the use of nonlinear optical effects in which the response of the bulk vanishes by symmetry.

We acknowledge Dan Parker, Joel Moore, Qimin Yan, and Mike Zdilla for useful conversations. J. O. was supported by the Quantum Materials program, Director, Office of Science, Office of Basic Energy Sciences, Materials Sciences and Engineering Division, of the U.S. Department of Energy under Contract No. DE-AC02-05CH11231. J. O. received support for optical measurements from the Gordon and Betty Moore Foundation's EPiQS Initiative through Grant No. GBMF4537 at UC Berkeley. The work at Temple University was funded by the National Science Foundation under Grant No. NSF/DMR-1945222. K. M. and C. F. acknowledge the financial support from the European Research Council (ERC) Advanced Grant No. 742068 TOP-MAT; European Unions Horizon 2020 research and innovation program (Grants No. 824123 and No. 766566) and Deutsche Forschungsgemeinschaft (DFG) through SFB 1143. K. M. acknowledges the Max Planck Society for the funding support under Max PlanckIndia partner group project. R. O. acknowledges funding from SRC ACSENT program and Turkish Fulbright Commission.

*These two authors contributed equally to this work.
†jworenstein@lbl.gov
‡dtorchin@temple.edu

[1] M. Z. Hasan and C. L. Kane, Rev. Mod. Phys. **82**, 3045 (2010).
[2] X.-L. Qi and S.-C. Zhang, Rev. Mod. Phys. **83**, 1057 (2011).
[3] L. Fu, C. L. Kane, and E. J. Mele, Phys. Rev. Lett. **98**, 106803 (2007).
[4] D. Hsieh, D. Qian, L. Wray, Y. Xia, Y. S. Hor, R. J. Cava, and M. Z. Hasan, Nature (London) **452**, 970 (2008).
[5] X. Wan, A. M. Turner, A. Vishwanath, and S. Y. Savrasov, Phys. Rev. B **83**, 205101 (2011).
[6] N. P. Armitage, E. J. Mele, and A. Vishwanath, Rev. Mod. Phys. **90**, 015001 (2018).
[7] S.-Y. Xu, C. Liu, S. K. Kushwaha, R. Sankar, J. W. Krizan, I. Belopolski, M. Neupane, G. Bian, N. Alidoust, T.-R. Chang, H.-T. Jeng, C.-Y. Huang, W.-F. Tsai, H. Lin, P. P. Shibayev, F.-C. Chou, R. J. Cava, and M. Z. Hasan, Science **347**, 294 (2015).
[8] B. Q. Lv, H. M. Weng, B. B. Fu, X. P. Wang, H. Miao, J. Ma, P. Richard, X. C. Huang, L. X. Zhao, G. F. Chen, Z. Fang, X. Dai, T. Qian, and H. Ding, Phys. Rev. X **5**, 031013 (2015).
[9] S.-Y. Xu, I. Belopolski, N. Alidoust, M. Neupane, G. Bian, C. Zhang, R. Sankar, G. Chang, Z. Yuan, C.-C. Lee, S.-M. Huang, H. Zheng, J. Ma, D. S. Sanchez, B. Wang, A. Bansil, F. Chou, P. P. Shibayev, H. Lin, S. Jia, and M. Z. Hasan, Science **349**, 613 (2015).
[10] I. Belopolski, S.-Y. Xu, D. S. Sanchez, G. Chang, C. Guo, M. Neupane, H. Zheng, C.-C. Lee, S.-M. Huang, G. Bian, N. Alidoust, T.-R. Chang, B. K. Wang, X. Zhang, A. Bansil, H.-T. Jeng, H. Lin, S. Jia, and M. Z. Hasan, Phys. Rev. Lett. **116**, 066802 (2016).
[11] H. Inoue, A. Gyenis, Z. Wang, J. Li, S. W. Oh, S. Jiang, N. Ni, B. A. Bernevig, and A. Yazdani, Science **351**, 1184 (2016).
[12] A. C. Potter, I. Kimchi, and A. Vishwanath, Nat. Commun. **5**, 5161 (2014).
[13] P. J. W. Moll, N. L. Nair, T. Helm, A. C. Potter, I. Kimchi, A. Vishwanath, and J. G. Analytis, Nature (London) **535**, 266 (2016).
[14] S. Jia, S.-Y. Xu, and M. Z. Hasan, Nat. Mater. **15**, 1140 (2016).
[15] L.-K. Shi and J. C. W. Song, Phys. Rev. B **96**, 081410(R) (2017).
[16] J. C. W. Song and M. S. Rudner, Phys. Rev. B **96**, 205443 (2017).
[17] D. K. Mukherjee, D. Carpentier, and M. O. Goerbig, Phys. Rev. B **100**, 195412 (2019).
[18] S. Ghosh and C. Timm, Phys. Rev. B **101**, 165402 (2020).
[19] D. Wawrzik, J.-S. You, J. I. Facio, J. van den Brink, and I. Sodemann, Phys. Rev. Lett. **127**, 056601 (2021).

[20] Q. Ma, A. G. Grushin, and K. S. Burch, Nat. Mater. (2021), https://doi.org/10.1038/s41563-021-00992-7.
[21] J. Orenstein, J. Moore, T. Morimoto, D. Torchinsky, J. Harter, and D. Hsieh, Annu. Rev. Condens. Matter Phys. **12**, 247 (2021).
[22] G. Chang, S.-Y. Xu, B. J. Wieder, D. S. Sanchez, S.-M. Huang, I. Belopolski, T.-R. Chang, S. Zhang, A. Bansil, H. Lin, and M. Z. Hasan, Phys. Rev. Lett. **119**, 206401 (2017).
[23] P. Tang, Q. Zhou, and S.-C. Zhang, Phys. Rev. Lett. **119**, 206402 (2017).
[24] G. Chang, B. J. Wieder, F. Schindler, D. S. Sanchez, I. Belopolski, S.-M. Huang, B. Singh, D. Wu, T.-R. Chang, T. Neupert, S.-Y. Xu, H. Lin, and M. Z. Hasan, Nat. Mater. **17**, 978 (2018).
[25] F. Flicker, F. de Juan, B. Bradlyn, T. Morimoto, M. G. Vergniory, and A. G. Grushin, Phys. Rev. B **98**, 155145 (2018).
[26] C. Le, Y. Zhang, C. Felser, and Y. Sun, Phys. Rev. B **102**, 121111(R) (2020).
[27] Z. Ni, B. Xu, M.-Á. Sánchez-Martínez, Y. Zhang, K. Manna, C. Bernhard, J. W. F. Venderbos, F. de Juan, C. Felser, A. G. Grushin, and L. Wu, npj Quantum Mater. **5**, 96 (2020).
[28] H. Li, S. Xu, Z.-C. Rao, L.-Q. Zhou, Z.-J. Wang, S.-M. Zhou, S.-J. Tian, S.-Y. Gao, J.-J. Li, Y.-B. Huang, H.-C. Lei, H.-M. Weng, Y.-J. Sun, T.-L. Xia, T. Qian, and H. Ding, Nat. Commun. **10**, 5505 (2019).
[29] T. A. Cochran, G. Chang, I. Belopolski, K. Manna, D. S. Sanchez, Z. Chng, J.-X. Yin, H. Borrmann, J. Denlinger, C. Felser, H. Lin, and M. Z. Hasan, arXiv:2004.11365.
[30] D. S. Sanchez, I. Belopolski, T. A. Cochran, X. Xu, J. X. Yin, G. Chang, W. Xie, K. Manna, V. Süß, C. Y. Huang, N. Alidoust, D. Multer, S. S. Zhang, N. Shumiya, X. Wang, G. Q. Wang, T. R. Chang, C. Felser, S. Y. Xu, S. Jia, H. Lin, and M. Z. Hasan, Nature (London) **567**, 500 (2019).
[31] N. Sirica, R. I. Tobey, L. X. Zhao, G. F. Chen, B. Xu, R. Yang, B. Shen, D. A. Yarotski, P. Bowlan, S. A. Trugman, J.-X. Zhu, Y. M. Dai, A. K. Azad, N. Ni, X. G. Qiu, A. J. Taylor, and R. P. Prasankumar, Phys. Rev. Lett. **122**, 197401 (2019).
[32] Q. Ma, S.-Y. Xu, C.-K. Chan, C.-L. Zhang, G. Chang, Y. Lin, W. Xie, T. Palacios, H. Lin, S. Jia, P. A. Lee, P. Jarillo-Herrero, and N. Gedik, Nat. Phys. **13**, 842 (2017).
[33] G. B. Osterhoudt, L. K. Diebel, M. J. Gray, X. Yang, J. Stanco, X. Huang, B. Shen, N. Ni, P. J. Moll, Y. Ran, and K. S. Burch, Nat. Mater. **18**, 471 (2019).
[34] J. Liu, F. Xia, D. Xiao, F. J. García de Abajo, and D. Sun, Nat. Mater. **19**, 830 (2020).
[35] C.-K. Chan, N. H. Lindner, G. Refael, and P. A. Lee, Phys. Rev. B **95**, 041104(R) (2017).
[36] H. Plank, J. Pernul, S. Gebert, S. N. Danilov, J. König-Otto, S. Winnerl, M. Lanius, J. Kampmeier, G. Mussler, I. Aguilera, D. Grützmacher, and S. D. Ganichev, Phys. Rev. Mater. **2**, 024202 (2018).
[37] Y. Gao, S. Kaushik, E. J. Philip, Z. Li, Y. Qin, Y. P. Liu, W. L. Zhang, Y. L. Su, X. Chen, H. Weng, D. E. Kharzeev, M. K. Liu, and J. Qi, Nat. Commun. **11**, 720 (2020).
[38] E. L. Ivchenko and S. D. Ganichev, arXiv:1710.09223.
[39] F. de Juan, A. G. Grushin, T. Morimoto, and J. E. Moore, Nat. Commun. **8**, 15995 (2017).
[40] M.-A. Sánchez-Martínez, F. de Juan, and A. G. Grushin, Phys. Rev. B **99**, 155145 (2019).
[41] B. Bradlyn, J. Cano, Z. Wang, M. G. Vergniory, C. Felser, R. J. Cava, and B. A. Bernevig, Science **353**, aaf5037 (2016).
[42] D. Rees, K. Manna, B. Lu, T. Morimoto, H. Borrmann, C. Felser, J. E. Moore, D. H. Torchinsky, and J. Orenstein, Sci. Adv. **6**, eaba0509 (2020).
[43] L. Z. Maulana, K. Manna, E. Uykur, C. Felser, M. Dressel, and A. V. Pronin, Phys. Rev. Research **2**, 023018 (2020).
[44] G. Chang, J.-X. Yin, T. Neupert, D. S. Sanchez, I. Belopolski, S. S. Zhang, T. A. Cochran, Z. Chéng, M.-C. Hsu, S.-M. Huang, B. Lian, S.-Y. Xu, H. Lin, and M. Z. Hasan, Phys. Rev. Lett. **124**, 166404 (2020).
[45] See Supplemental Material at http://link.aps.org/supplemental/10.1103/PhysRevLett.127.157405 for material growth description, material symmetry analysis, experimental details, x-ray data, AFM data, and additional CPGE data.
[46] F. D. J. Brunner, J. A. Johnson, S. Grübel, A. Ferrer, S. L. Johnson, and T. Feurer, J. Opt. Soc. Am. B **31**, 904 (2014).
[47] J. A. Johnson, F. D. J. Brunner, S. Grübel, A. Ferrer, S. L. Johnson, and T. Feurer, J. Opt. Soc. Am. B **31**, 1035 (2014).
[48] H. Flack, Acta Crystallogr. Sect. A **39**, 876 (1983).
[49] J. C. H. Spence, J. M. Zuo, M. O'Keeffe, K. Marthinsen, and R. Hoier, Acta Crystallogr. Sect. A **50**, 647 (1994).
[50] C. Fang, L. Lu, J. Liu, and L. Fu, Nat. Phys. **12**, 936 (2016).
[51] Rescaling of the energy by a factor 1.25 can be obtained when DFT-LDA theory is augmented by inclusion of a certain amount of Hartree-Fock exchange using hybrid density functionals, for example in the Heyd, Scuseria, and Ernzerhof (HSE) approach. G. Chang and M. Z. Hasan, private communication (2021).

Supplementary Information for *Direct Measurement of Helicoid Surface States in RhSi using Nonlinear Optics*

Dylan Rees[1,2,*], Baozhu Lu[3,*], Yue Sun [2,4] Kaustuv Manna[5,6], Rüstem Özgür[7], Sujan Subedi[3]
Horst Borrmann[5] Claudia Felser[5], J. Orenstein[1,2†], Darius H. Torchinsky[3‡],

[1]Department of Physics, University of California, Berkeley, California 94720, USA

[2]Materials Science Division, Lawrence Berkeley National Laboratory Berkeley, California 94720, USA

[3]Department of Physics, Temple University, Philadelphia, Pennsylvania 19122, USA

[4]Department of Chemistry, University of California, Berkeley, California 94720, USA

[5]Max Planck Institute for Chemical Physics of Solids, Dresden, D-01187, Germany

[6]Department of Physics, Indian Institute of Technology Delhi, New Delhi 110016, India

[7]Department of Materials Science and Engineering, University of California, Berkeley, CA 94720, USA.

[*] These authors contributed equally.

† jworenstein@lbl.gov

‡dtorchin@temple.edu

Supplementary Text

Crystal Growth and Structure Refinement

Single crystal of RhSi was grown using a self-flux technique from a critical non-stoichiometric composition. Here we induced slightly excess Si to ensure a flux growth inside the Bridgman ampule. First, a polycrystalline ingot was prepared by pre-melting the highly pure metals under argon atmosphere using an arc furnace. Then the crushed powder was filled in an alumina tube and finally sealed inside a tantalum tube with argon atmosphere. The sample was heated to 1500 °C in a tubular furnace kept inside a glove box with argon atmosphere. Then the furnace was slowly cooled with 1 °C/h up to 1200 °C and finally rapidly cooled to room temperature by switching-off the furnace. High quality single crystal was grown with average dimension of $\sim$ 10 mm length and $\sim$ 6 mm diameter. The single crystallinity was first checked with a white beam backscattering Laue X-ray setup at room temperature. Stoichiometric composition was confirmed with energy-dispersive X-ray (EDX) spectroscopy measurements. A small piece was broken from the large crystal and selected fragments were mounted on Kapton loops and tested for structure refinement. Data were collected on a Rigaku AFC7 four-circle diffractometer with a Saturn 724+ CCD-detector applying graphite-monochromatized Mo-Kα radiation. Pertinent details are given in Table 1, complete crystallographic information has been deposited and is available citing CSD-2111732. Fig. S1 shows an oscillation image of the RhSi single crystal, confirming high crystal quality, along with pictures of various single crystal batches. Fig. S2 shows the crystal structure of RhSi.

Laue diffraction data used to orient the [100] and [010] axes within the surface along with the predicted peaks of space group 198 are shown in Fig. S3. Measurements were performed at the Advanced Light Source at Lawrence Berkeley National Laboratory.

Table 1: Room temperature single crystal Refinement result for RhSi.

Formula	RhSi
F.W. (g/mol);	131
Space group; Z	P213 (No. 198); 4
a (Å)	4.6858(9)
V (Å^3)	102.88(6)
Absorption Correction	Multi-scan
Extinction Coefficient	0.22(1)
θ range (°)	6.1-51.3
No. reflections; Rint	5013; 0.0341
No. independent reflections	392
No. parameters	9
R1; wR2 (all I)	0.0132; 0.0341
Goodness of fit	2.410
Diffraction peak and hole (e-/Å^3)	0.760; -1.147

Material Symmetries

1. Nonlinear Tensor

The second-order optical nonlinearity generates currents at both the sum and difference frequencies of the applied electric field. LPGE and CPGE correspond to the current generated at the difference frequency,

$$J_i = \sigma_{ijk} E_j E_k^* \tag{1}$$

For cubic space group $P2_13$ the only nonvanishing elements of σ_{ijk} have indices xyz and permutations. The elements with even permutations of xyz are equal to σ_{xyz} and odd permutations are equal to σ^*_{xyz}. If we write $\sigma_{xyz} = \gamma + i\beta$ where γ and β are both real, the structure of the third rank tensor can be written in the form

$$\sigma^{(2)} = \begin{pmatrix} \begin{pmatrix} 0 \\ 0 \\ 0 \end{pmatrix} & \begin{pmatrix} 0 \\ 0 \\ \gamma + i\beta \end{pmatrix} & \begin{pmatrix} 0 \\ \gamma - i\beta \\ 0 \end{pmatrix} \\ \begin{pmatrix} 0 \\ 0 \\ \gamma - i\beta \\ 0 \\ \gamma + i\beta \\ 0 \end{pmatrix} & \begin{pmatrix} 0 \\ 0 \\ 0 \end{pmatrix} & \begin{pmatrix} \gamma + i\beta \\ 0 \\ 0 \end{pmatrix} \\ \begin{pmatrix} \gamma - i\beta \\ 0 \\ 0 \end{pmatrix} & \begin{pmatrix} 0 \\ 0 \\ 0 \end{pmatrix} \end{pmatrix} \tag{2}$$

where the element σ_{ijk} is the kth element of the column vector in the ith row and jth column of the outer matrix.

2. PGEs at normal incidence

For light incident on the [001] face, there will only be generated 2nd order effects when the electric field has nonzero components in x and y. Eq. 1 gives $J_z \propto E_x E_y$ and $J_x = J_y = 0$. As currents directed in z have radiation patterns that become zero in the z direction, no radiation will be measured by exciting second order bulk currents at normal incidence on the [001] face.

3. Transformation properties of the CPGE

The circular photogalvanic current can be written in terms of the photon helicity,

$$J_i = \beta_{ij}(\mathbf{E} \times \mathbf{E}^*)_j. \tag{3}$$

The second rank CPGE tensor is contracted from the third-rank conductivity tensor according to the relation,

$$\beta_{ij} = \sigma_{ikl}\epsilon_{jkl}, \tag{4}$$

where ϵ_{jkl} is the unit antisymmetric tensor. Substitution of the conductivity tensor for the RhSi space group (Eq. 2) yields,

$$\beta_{ij} = i\beta\delta_{ij}, \tag{5}$$

where δ_{ij} is the Kronecker delta. The factor of i before β is the imaginary unit. Substitution into Eq. 3 yields,

$$\mathbf{J} = i\beta\mathbf{E} \times \mathbf{E}^*, \tag{6}$$

which shows that for the case of space group $P2_13$ the CPGE current is always directed parallel to the helicity vector, regardless of its direction with respect to the crystal axes. This means that CPGE polarization that depends on crystal orientation, as reported in the main text, breaks the constraints imposed by bulk symmetry. Additional CPGE spectra on two sample are shown in Fig. S4.

4. Fitting LPGE data to nonlinear tensor element parameters

Vertical and horizontal terahertz pulses are measured as a function of pump wavelength and pump linear polarization angle. For a general nonlinear LPGE tensor γ_{ijk}, illuminating a medium with linear polarization light with electric field $\mathbf{E}$ gives photogalvanic current components

$$J_i = \gamma_{ijk}E_jE_k \tag{7}$$

assuming $\mathbf{E}$ has linear polarization (i.e. the components of $\mathbf{E}$ have zero relative complex phase).

4.1 Sources of Experimental Error

Both THz polarizations were acquired at each pump wavelength before the wavelength was changed. This required that the ZnTe crystal and THz polarizer be adjusted to select for the horizontal and vertical emitted THz polarizations in turn. In the optical biasing scheme used here [1, 2], this resulted in a small difference in the measured THz amplitude as the probe and THz beams passed through slightly different positions on the ZnTe detection crystal each time it was rotated. Through repeated measurements, we estimate that this error was, on average, $\sim \pm 7.5\%$ of the total THz amplitude. We have accounted for this error with error bars on the plots of the LPGE parameters.

4.2 Pump polarization rotation

In the set of LPGE experiments, we rotate the pump polarization while the sample remains fixed, and the electric field is given by $\mathbf{E}(\theta) = E_0(\cos\theta, \sin\theta)$. This gives photogalvanic currents

$$J_x = \left(\gamma_{xxx}\cos^2\theta + \gamma_{xyy}\sin^2\theta + 2\gamma_{xxy}\cos\theta\sin\theta\right)E_0^2$$

$$J_y = \left(\gamma_{yxx}\cos^2\theta + \gamma_{yyy}\sin^2\theta + 2\gamma_{xyy}\cos\theta\sin\theta\right)E_0^2. \tag{8}$$

For each pump wavelength and terahertz polarization, the set of data has three free parameters, illustrated simply by a sine wave plus an offset with parameters A, ϕ and C: $A\sin(2\theta+\phi)+C$. Thus, for two terahertz polarizations, we have six free variable and can thus determine the tensor parameters γ_{ijk} for $ijk = xxx, xxy, xyy, yxx, yxy, yyy$. Note that $\gamma_{ixy} = \gamma_{iyx}$. Data for multiple wavelengths is shown in Fig. S5.

4.3 Sample rotation

We can determine the same set of six parameters by keeping the pump polarization fixed at $\theta = 0$ and instead rotating the sample axis about the surface normal by angle η. The two terahertz components measured will be

$$J_x(\eta) = \left(\gamma_{xxx}\cos^3\eta - (\gamma_{xxy}+\gamma_{xyx}+\gamma_{yxx})\cos^2\eta\sin\eta + (\gamma_{xyy}+\gamma_{yxy}+\gamma_{yyx})\cos\eta\sin^2\eta - \gamma_{yyy}\sin^3\eta\right)E_0^2 \tag{9}$$

and

$$J_y(\eta) = \left(\gamma_{yxx}\cos^3\eta + (\gamma_{xx}-\gamma_{yxy}-\gamma_{yyx})\cos^2\eta\sin\eta + (\gamma_{yyy}-\gamma_{xxy}-\gamma_{xyx})\cos\eta\sin^2\eta - \gamma_{xyy}\sin^3\eta\right)E_0^2. \tag{10}$$

This allows us to use two different measurement methods to determine the same set of parameters γ_{iyx}.

5. In-plane mirror symmetry

Consider a general nonlinear tensor σ that describes the optical response in a material such that $J_i = \sigma_{ijk}E_iE_k$. We will consider the constrains on σ imposed by a symmetry of the mirror operation

$$M^x = \begin{pmatrix} -1 & 0 \\ 0 & 1 \end{pmatrix} \tag{11}$$

where, whithout loss of generality, we are restricting ourselves to 2D.

Under an operator $\mathcal{O}$, σ will transform as

$$\sigma'_{ijk} = \mathcal{O}_{i\alpha}\mathcal{O}_{j\beta}\mathcal{O}_{k\gamma}\sigma_{\alpha\beta\gamma}. \tag{12}$$

When $\mathcal{O}$ is a symmetry of the material in question, the constraint $\sigma'_{ijk} = \sigma_{ijk}$ is imposed. For $\mathcal{O} = M^x$, we arrive at the set of equations

$$\begin{aligned}
\sigma'_{xxx} &= \quad (M^x_{xx})^3\sigma_{xxx} = -\sigma_{xxx} = \sigma_{xxx} \quad (*)\\
\sigma'_{xxy} &= (M^x_{xx})^2M^x_{yy}\sigma_{xxy} = \quad \sigma_{xxy} = \sigma_{xxy}\\
\sigma'_{xyy} &= M^x_{xx}(M^x_{yy})^2\sigma_{xyy} = -\sigma_{xyy} = \sigma_{xyy} \quad (*)\\
\sigma'_{yxx} &= (M^x_{xx})^2M^x_{yy}\sigma_{yxx} = \quad \sigma_{yxx} = \sigma_{yxx}\\
\sigma'_{xyy} &= M^x_{xx}(M^x_{yy})^2\sigma_{yxy} = -\sigma_{yxy} = \sigma_{yxy} \quad (*)\\
\sigma'_{yyy} &= \quad (M^x_{yy})^3\sigma_{yyy} = \quad \sigma_{yyy} = \sigma_{yyy}
\end{aligned} \tag{13}$$

The starred equations indicate elements that we find are equal to their own negative and therefore must be zero. We can conclude that for mirror symmetry under M^x, the elements σ_{xxx}, σ_{xyy} and σ_{yxy} must be zero.

AFM

We performed atomic force microscopy (AFM) measurements over two 5×5 μm^2 regions and two 1×1 μm^2 regions (Fig. S6). We find no patterns in the surface topography which could define any overall preferred direction in optical measurements. A surface variation of approximately 5 nm is observed.

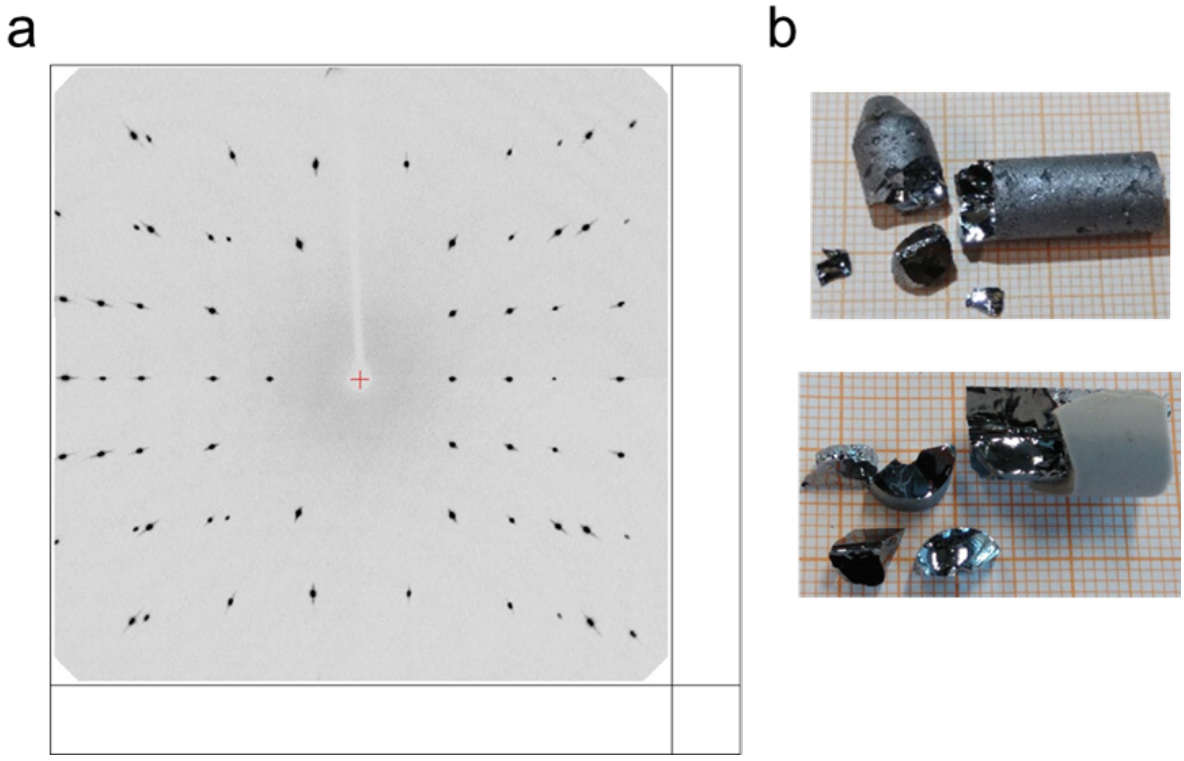

Fig. S1. (a) Oscillation image about the b-axis of the RhSi single crystal confirming high crystal quality (left). (b) Pictures of various RhSi single crystal batches (right).

Reproducibility

CPGE spectra from samples deriving from two different growth batches are shown in Fig. S4. The x component of the current is shown in panel (a) while the y component of the current is shown in panel (b). The data were taken from two different points on the surface of sample A and three different points on the surface of sample B, while only the idler range of the OPA ($\sim$ 475 - 785 meV) was used for most of the traces in order to maintain consistent optical alignment while capturing the bulk of the CPGE response. The spectra are extremely reproducible, with the small difference in magnitude and lineshape between the various j_y traces due to imprecision in aligning the crystal axes to the lab frame axes in between individual data scans, which can slightly mix j_x into j_y. The data for the main text where chosen based on the superior signal-to-noise ratio of THz transients and the resulting spectrum.

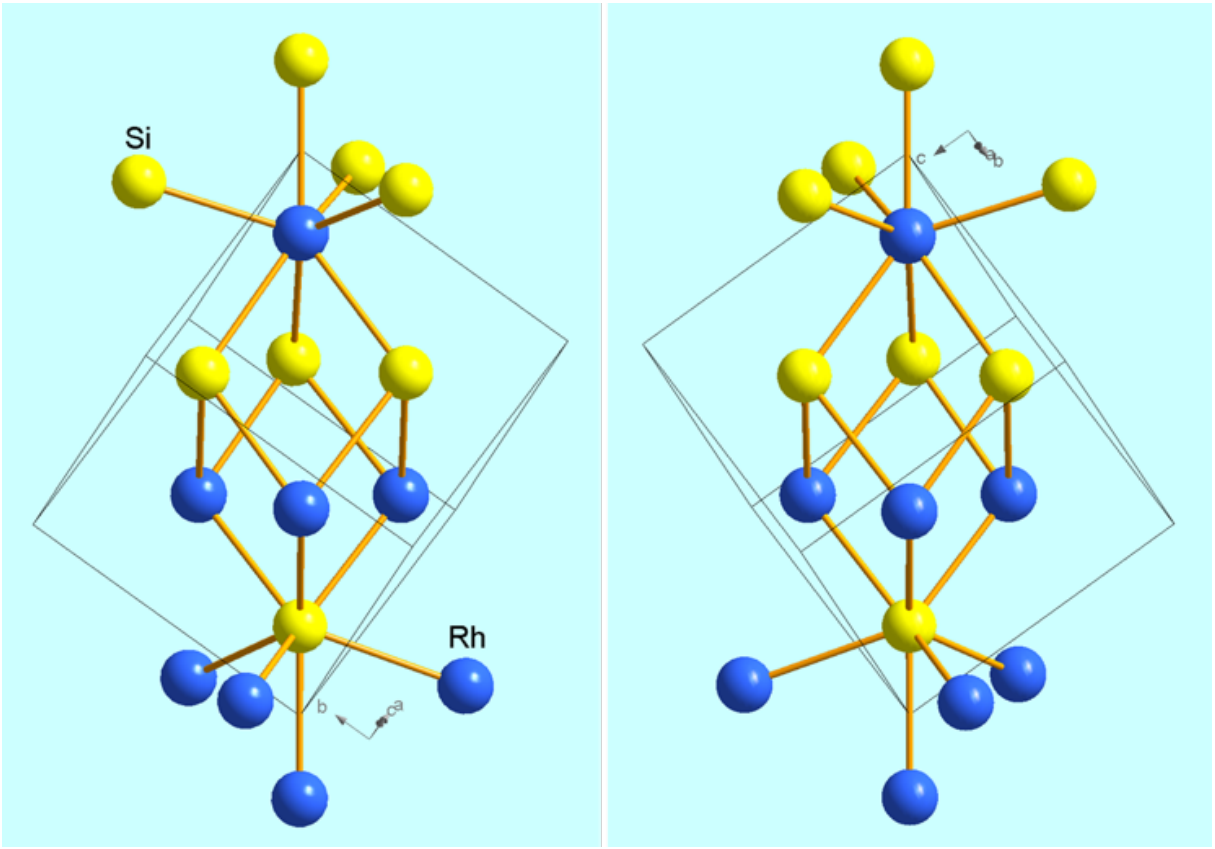

Fig. S2. Atomic arrangement as refined for RhSi single crystal. Both atoms occupy Wyckoff position 4a (x,x,x) with Rh at x = 0.85314(3) and Si at x = 0.15846(12). The Flack parameter refined to: -0.06(4) and thus confirms the proper assignment of the absolute structure (left). For the inverted structural model depicted on the right Flack parameter refined to +1.03(4), i.e., corroborating proper assignment without contributions from twinning by inversion. The atomic arrangements are in accordance with form B as assigned for FeSi type structures [3]. Results for crystals selected from a second batch single crystal are also in perfect agreement.

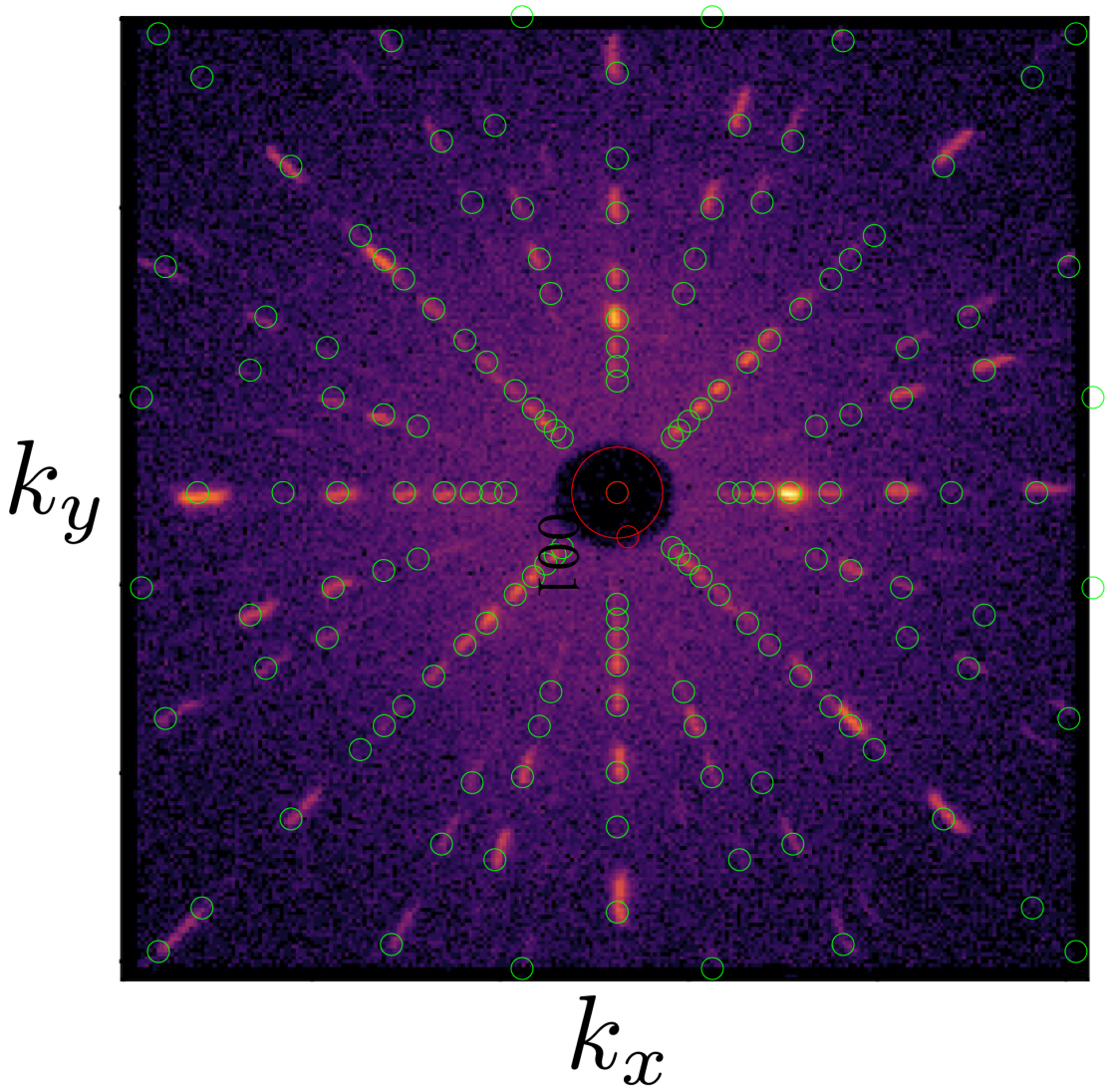

Fig. S3. Laue diffraction measurement overlaid with the predicted diffraction peaks of the 001 surface of space group 198.

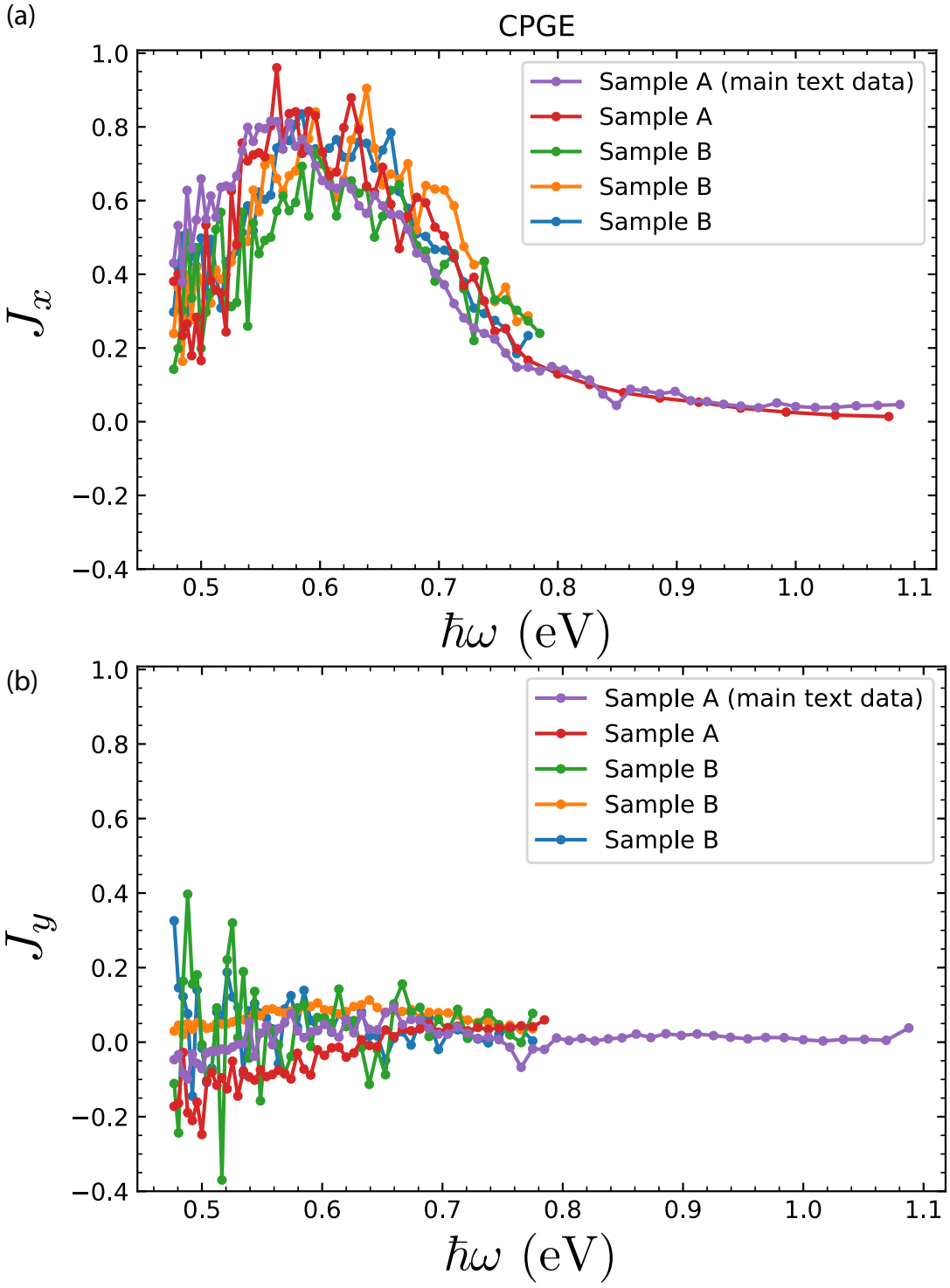

Fig. S4. Additional CPGE scans with (a) horizontal polarization and (b) vertical polarization.

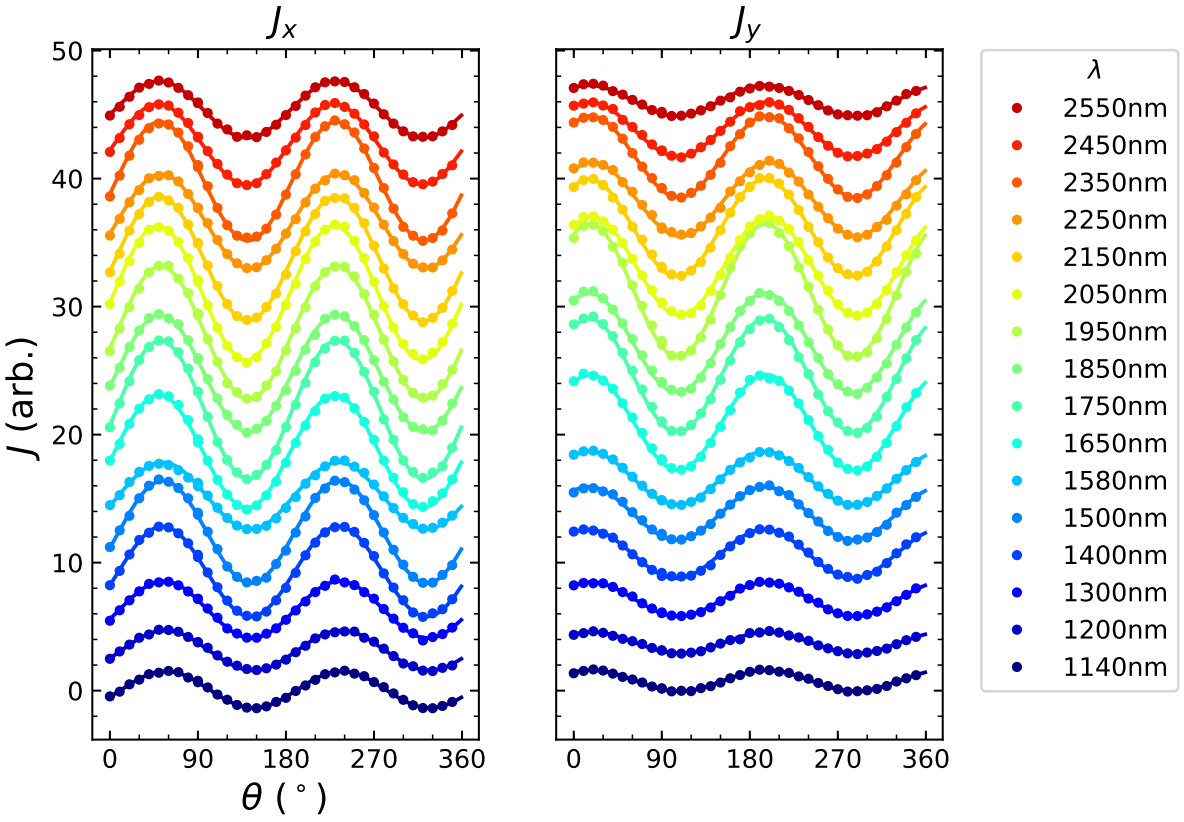

Fig. S5. LPGE measurements on RhSi 001 surface as a function of pump polarization angle for x and y components of terahertz.

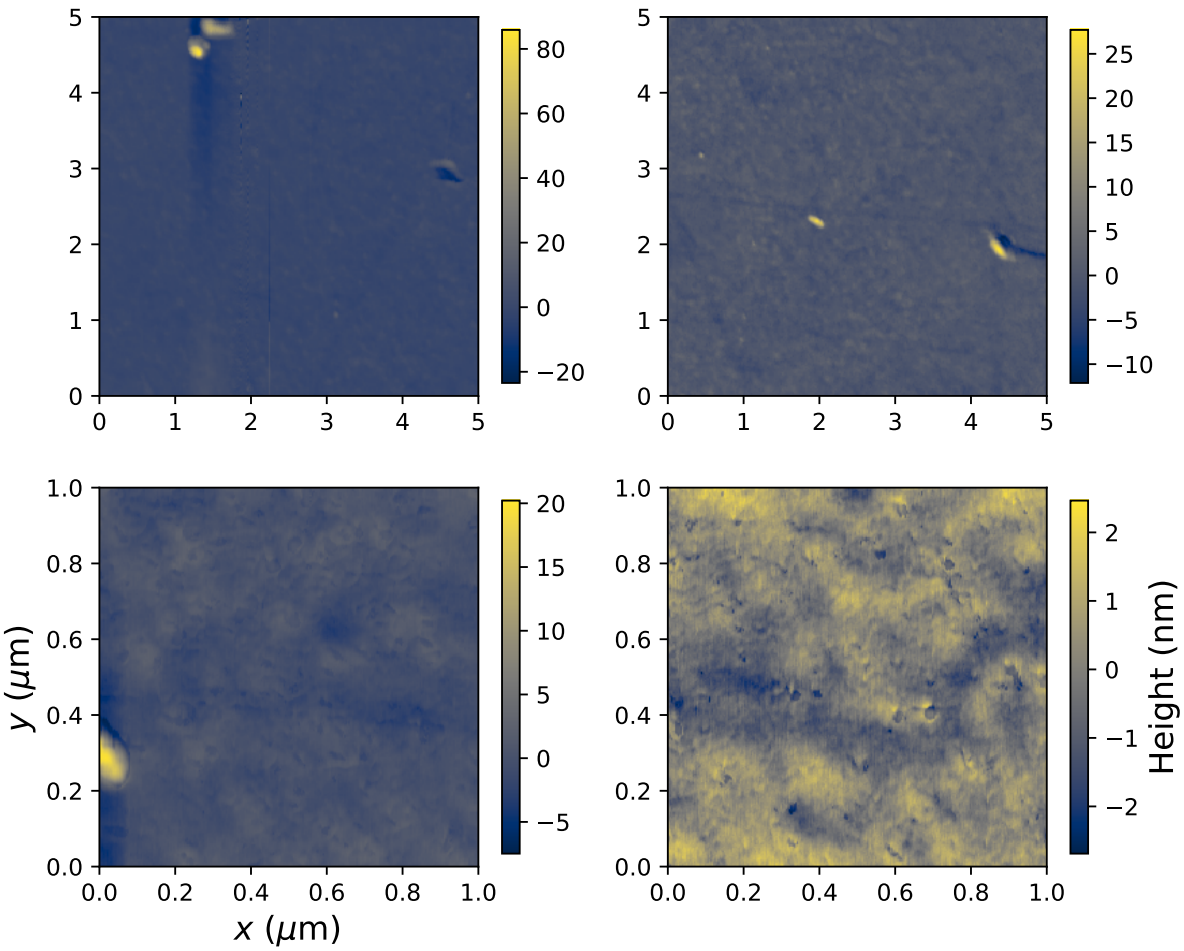

Fig. S6. Four AFM measurements on RhSi [001] surface showing crystal topography.

References

[1] F. D. J. Brunner, J. A. Johnson, S. Grübel, A. Ferrer, S. L. Johnson, and T. Feurer. Distortion-free enhancement of terahertz signals measured by electro-optic sampling. i. theory. *J. Opt. Soc. Am. B*, 31(4):904–910, Apr 2014.

[2] J. A. Johnson, F. D. J. Brunner, S. Grübel, A. Ferrer, S. L. Johnson, and T. Feurer. Distortion-free enhancement of terahertz signals measured by electro-optic sampling. ii. experiment. *J. Opt. Soc. Am. B*, 31(5):1035–1040, May 2014.

[3] J. C. H. Spence, J. M. Zuo, M. O'Keeffe, K. Marthinsen, and R. Hoier. On the minimum number of beams needed to distinguish enantiomorphs in X-ray and electron diffraction. *Acta Crystallographica Section A*, 50(5):647–650, Sep 1994.